Condensed Matter Physics, 2004, Vol. 7, No. 1(37), pp. 79–100

CONDENSED MATTER PHYSICS

Tight-binding description of TiC_x

V.I.Ivashchenko [1], P.E.A.Turchi [2], V.I.Shevchenko [1], L.A.Ivashchenko [1], O.K.Porada [1]

[1] Institute of Problems of Material Science, NAS of Ukraine, Krzhyzhanovsky Str. 3, 03142 Kyiv, Ukraine

[2] Lawrence Livermore National Laboratory (L-353), P.O. Box 808, Livermore, CA 94551, USA

Received December 8, 2003

A parametrized non-orthogonal tight-binding (TB) method combined with the coherent-potential-approximation is applied to the study of the electronic structure of disordered off-stoichiometric TiC_x, the lattice relaxation and the electronic spectra of the TiC (001) surface, the local relaxation and energetic states of TiC structures with one or two vacancies in both the non-metal and metal sublattices. The calculated results are in good agreement with available experimental and theoretical data. The importance of the overlap matrix elements of the TB Hamiltonian in describing the electronic structure of this class of compounds is emphasized.

Key words: *titanium carbide, non-orthogonal tight-binding model, single vacancy, surface relaxation*

PACS: *71.20.B, 61.72.J, 68.35.B*

1. Introduction

Titanium carbide in the rock-salt structure (NaCl-type) exhibits unique features that are of interest for both experimental and theoretical investigations [1]. Experimental evidence shows that there can be large amounts of vacancies on the non-metal sublattice, while the metal sublattice can only contain single vacancies [1–3], thus leading to possible large deviations from stoichiometry. Experimentally the lattice parameter (a) for TiC_x expands for $0.9 < x < 1.0$ and shrinks for $0.48 < x < 0.9$, the total change in lattice parameter being less than $1\,\%$ [1,2]. For a certain range of composition, the cubic phase seems to be thermodynamically stable solely at high temperatures. Several off-stoichiometric ordered structures of TiC_x have been reported and investigated in the range of $0.48 < x < 0.96$ [4–6]. In particular, the existence of at least two vacancy-ordered structures, the cubic and trigonal forms of hemicarbide Ti_2C, is now well established experimentally [4,5]. On the other hand, the non-metal vacancies show some short-range order [6].

The electronic structure of TiC_x was carefully studied by using different experimental procedures. The results of these studies have been reviewed in [3]. The main consequence of C-vacancies was the existence of additional metal states in the density of states (DOS) minimum.

Most of the experimental studies on the static atomic relaxation around vacancies in TiC_x and other transition metal carbides and nitrides point to an outward relaxation of the metal atoms located around a non-metal vacancy [7–11]. In particular, in TiC_x, for $0.6 < x < 0.94$ the outward relaxations of about $0.03 - 0.097$ Å of the first nearest neighbors of the C-vacancy were established. It was also found that the magnitude of the outward relaxation is strongly dependent on the stoichiometry, i.e., the more vacancy neighbors a titanium atom has, the larger the relaxation is towards the remaining carbon atoms [4]. There is one reference in which a shift of the metal atoms towards the non-metal vacancy was found [12].

Titanium carbide is increasingly used as protective coatings for cutting tools, as its renowned hardness can lead to a considerable improvement in tribological performance. One primary limiting factor in these high-stress applications is the brittleness of TiC that cleave on a (001) plane. In this connection, it is important to know a character of the atomic relaxation on this surface plane. As far as the authors know, the relaxation of TiC (001) was experimentally studied only by Aono et al. [13]. The authors of this study concluded that this surface does not exhibit any rumpling relaxation within ± 0.1 Å [13]. The electronic structure of the TiC (001) surface was studied by means of angle-resolved photo-emission spectroscopy [14,15], and, it was shown, in particular, that the TiC (001) spectrum resembles the bulk one. Here it should be noted that other experiments on the TiN (001) [16] have clearly revealed surface levels located about 0.07 Ryd above the main peak.

Various theoretical attempts have been made to explain the above mentioned experimental findings of both stoichiometric [17–34] and off-stoichiometric [35–46] titanium carbides. We classify the recent theoretical works devoted to the study of TiC_x in table 1. In the present work we will focus on the possibility for the non-metal sublattice to display full randomness [35–37]. Here we stress that despite a lot of the band structure calculations of the ordered substoichiometric titanium carbides (table 1), they are not able to explain the experimental results related to the Fermi surface and the density of states (DOS) at the Fermi level (E_{F}). It is well known that vacancy ordering causes the appearance of a thin structure in the DOS. Such a DOS structure makes difficult the analysis of changes in the DOS at E_{F} as a function of vacancy concentration. Therefore, to correctly investigate the DOS of randomized TiC_x, depending on x, it is necessary to employ a method based on the effective medium approximation. Klima [36] has applied an orthogonal TB-coherent potential approximation (CPA) procedure to calculate the DOS of TiC_x. His results did not reveal any vacancy states. Later, by applying the Korringa-Kohn-Rostoker (KKR)-CPA approach, Marksteiner et al. [37] have shown that the introduction of C-vacancies in TiC leads to the appearance of a vacancy peak that broadens and shifts to higher energies with the increasing vacancy concentration. Because of the non self-consistency of the potentials used [37], for TiC_x there is an artificial bump

Table 1. Theoretical investigations of the electronic structure, phase stability, structural relaxation of TiC_x by using different methods. Abbreviations: FP – Full-Potential; LMTO – Linear Muffin-Tin Orbitals; APW – Augmented Plane Wave; ASA – Atomic Sphere Approximation; PP – Pseudopotential; KKP – Korringa-Kon-Rostoker; CPA – Coherent Potential Approximation; ATA – Average T-matrix Approximation; TB – Tight Binding; MC – Monte Carlo.

$TiC_{1.0}$	TiC_x disordered	TiC_x ordered
$[17-26]^a$	[35], KKP-ATA	[25], FP-LMTO
[23], FP-LMTO	[36], TB-CPA	[26], FP-LAPW
[25], FP-LMTO	[37], KKR-CPA	[38], RM
[27], APW		[39, 40], APW
[28], LMTO-ASA		[28, 30, 41, 42], LMTO-ASA
[29], LMTO		[30, 43], TB-LMTO
[30], TB-LMTO		[44], TB
[31 – 34], PP		[45], MC, FP-LMTO

TiC_x $x < 0.95$	TiC(001)
[25], FP-LMTO	[47], TB
[44], TB	[48, 49], FP-LAPW
[46], CLUSTER	[51 – 53], FP-LMTO
	[50], TB
	[54], PP

[a] Review articles, or the articles in which a short review on the problem has been made.

in the DOS at E_F. Besides, the calculations [37] were performed in a very narrow energy range around E_F.

The rearrangement of the atomic configuration in TiC_x caused by the presence of the non-metal vacancies was theoretically studied by using different procedures [25,26,44,46] (table 1). The results predicted an outward shift of the metal atoms near the vacancy of 0.107 Å for the single vacancy in the Ti_6C_{18} cluster [46], 0.049 Å for $TiC_{0.88}$ and 0.08 Å for $TiC_{0.5}$ [25], 0.100 Å for TiC_x, $x = 1.0-0.5$ [44] and 0.038 Å for $TiC_{0.5}$ [26]. It was found that, for the ordered phases, the atomic shift increases with increasing a vacancy concentration, which is consistent with the experimental results [4]. However, if one takes into account that the experimental values of the outward relaxation are 0.03 Å for ordered $TiC_{0.76}$ [7], 0.05 Å for $TiC_{0.64}$ and $TiC_{0.76}$ [9] and 0.07 Å for ordered $TiC_{0.6}$ [10], one can see that the theoretical calculations overestimate the atomic shift (with the exception of the calculation [26] that predicts the shift of 0.038 Å for ordered $TiC_{0.5}$). The value of 0.097 Å obtained from X-ray diffraction measurements on $TiC_{0.94}$ also contradicts the above mentioned experimental regularity [8]. So, from these considerations it follows that there are discrepancies between theoretical and experimental results on the value of the outward relaxation in TiC_x, especially for small x. Hugosson et al. [25] did not find the theoretical confirmation of the expansion of the lattice parameter for TiC_x, for $x < 0.9$, while Tan et al. [44] found a small expansion or contraction of the lattice parameter, depending on the choice of vacancy positions.

The non-orthogonal TB method with a restricted basis (C s, C p and Ti d functions) [47] and the full-potential linearized augmented plane wave (FP-LAPW) method [48,49] were applied to the study of the TiC (001) surface represented by a five-layer slab. Based on both methods, the layer projected DOS shows a surface-induced high-energy shift of about 0.050 Ryd [47] and 0.036 Ryd [49]. Associated with this shift is the formation of surface resonance states (SRS). Note that, for the calculation of the DOS of the (001) surface, atomic relaxations within the slabs were not considered. Later [50], the TB investigation of the TiC(001) surface have showed that the metal atoms are displaced outwards and the carbon inwards in agreement with the prediction of Wimmer et al. [49]. However, more resent investigations based on FP-LMTO [51–53] and pseudopotential [54] approaches give the opposite rumpling relaxation. The value of the rumpling relaxation in all the calculations is consistent with that found from the experiment [13].

The short review of the experimental and theoretical investigations on TiC_x, showing the advantages and shortcomings of different theoretical approaches, enables us to formulate the main tasks of the present study that are in the following.

- To obtain more complete information about the effect of the non-metal vacancies on the electronic structure in randomized TiC_x in the wide energy and concentration ranges.
- To investigate the lattice relaxation in titanium carbides containing single non-metal and metal vacancies, two non-metal vacancies in different configurations.
- To study the atomic and electronic structures of the relaxed TiC (001) surface as well as the atomic relaxation inside a multi-layered slab.

For this purpose we use a modified non-orthogonal tight-binding (NTB) interpolation scheme, which is applied in combination with the CPA to perform total energy calculations. In this model, the repulsive contribution to the total energy was parametrized from the results of total energy (E_{T}) obtained within a first-principles pseudo-potential method. The efficiency of the suggested approach is corroborated by the comparison of our results with the experiment and other theoretical findings.

The paper is organized as follows. In section 2 we comment on the theoretical procedures, and, in particular, on the choice of basis functions within the TB approach. In section 3 we present and discuss the results of: a) DOS of stoichiometric and off-stoichiometric titanium carbide in a wide energy range; b) atomic relaxations in several coordination shells around the non-metal (V_{C}) and the metal (V_{Ti}) vacancies; c) atomic relaxations occurring in an 11-layer slab to establish the character of the relaxation caused by the presence of a surface; d) layer-projected DOS for the slab. Finally, section 4 contains the main conclusions.

2. Computational aspects

2.1. Determination of the parameters of the NTB interpolation scheme

To investigate complex systems with a large number of atoms in the unit cell we select the non-orthogonal TB interpolation scheme, originally suggested by Mattheiss [55] for transition metal compounds and adapted by Faulkner for calculating off-stoichiometric compositions [56]. Note that Papaconstantopoulos et al. [57] and Klima [36,58] have used a simpler, and less realistic orthogonal TB scheme that

Table 2. Parameters of the TB model. The notation of the two-center parameters is in accordance with [55]. The two-center parameters are given for the equilibrium distance $r = R_0$, and away from R_0, have to be multiplied by the factor $(R_0/r)^n$.

Notat.	C–C Param. (Ryd)	C–C n	C–Ti Param. (Ryd)	C–Ti n	Ti–Ti Param. (Ryd)	Ti–Ti n
One-center parameters						
E_s	0.14230				1.14177	
E_p	0.78957				1.35433	
E_{xy}					0.77231	
E_{3z}					0.72021	
Two-center hopping parameters						
$ss\sigma$	0.01266	2.0	–0.09095	1.63560	–0.08267	2.0
$sp\sigma$			–0.07920	1.63560	–0.11230	2.0
$sd\sigma$			–0.07404	2.86230	–0.05063	3.5
$ps\sigma$			–0.13188	1.63560	0.11230	2.0
$pp\sigma$	–0.01048	2.0	–0.10332	1.63560	0.14081	2.0
$pp\pi$	0.00495	2.0	0.00381	1.63560	–0.03640	2.0
$pd\sigma$			–0.02449	2.86230	0.07225	3.5
$pd\pi$			0.02901	2.86230	–0.02019	3.5
$ds\sigma$					–0.05063	3.5
$dp\sigma$					–0.07225	3.5
$dp\pi$					0.02019	3.5
$(dd\sigma)_1$					–0.04658	5.0
$(dd\pi)_1$					0.02139	5.0
$(dd\delta)_1$					–0.00054	5.0
$(dd\sigma)_2$					0.00675	5.0
$(dd\pi)_2$					–0.00194	5.0
$(dd\delta)_2$					0.00013	5.0
R_0 (Å)	3.013		2.131		3.013 (4.262)[a]	
R_{cut} (Å)	3.800		2.600		3.800 (4.800)[a]	

[a] The values in parenthesis correspond to the second nearest interactions.

neglected the role played by overlap matrix elements. In our approach, we use the extended non-orthogonal basis consisting of C s, C p, Ti s, Ti p and Ti d functions. The overlap of the functions is taken into account up to the first nearest neighbors (FNN). We consider the two-center approximation for the hoping and overlap integrals. The hopping integrals are calculated up to the second nearest neighbors (SNN). To improve the accuracy of the initial spectrum we have also included the d_{Ti}-d_{Ti} interaction associated with the next nearest neighbor atoms. When the parameters of the interpolation scheme are fitted, it is very important to know the symmetry of each eigenvalue in each k-point of the Brillouin zone (BZ) [55]. Therefore, we have chosen the spectrum of TiC calculated at 19 k-points of the BZ with a self-consistent non-linearized symmetrized APW method [27] for fitting. The TB Hamiltonian and overlap matrices at each k-point are presented in a block form. The TB eigenvalues belonging to a block correspond to the set of the APW eigenvalues with certain irreducible representation. In the non-linear least-square procedure we have used the APW eigenvalues from 11–12 valence energy bands. The root mean square and the maximum deviation of the APW and TB spectra were 0.0036 Ryd and 0.0123 Ryd, respectively, for all the eigenvalues and 0.0032 Ryd and 0.0067 Ryd, respectively, for $E < E_{\mathrm{F}}$. The parameters of the NTB interpolation scheme are listed in tables 2, 3.

Table 3. Two-center C–Ti overlap parameters of the NTB scheme. Notations are the same as in table 2.

Denotation	Parameters	n
$ss\sigma$	0.07626	0.02570
$sp\sigma$	0.12758	0.02570
$sd\sigma$	0.09253	0.06425
$ps\sigma$	0.05748	0.02570
$pp\sigma$	0.06764	0.02570
$pp\pi$	–0.06794	0.02570
$pd\sigma$	0.14457	0.06425
$pd\pi$	–0.04062	0.06425

2.2. TB-CPA procedure

The DOS of TiC_x with substitutional disorder on the non-metal sublattice are calculated in the framework of the NTB interpolation scheme combined with the single-site CPA as in the Faulkner scheme [56]. Two self-energies Σ_s and Σ_p associated with the carbon sites are determined iteratively [56]. The potentials of the empty sites are set equal to $+\infty$. Integrals over the BZ are replaced by a sum of diagonal elements of Green function computed at 916 k-points of the irreducible wedge of the BZ with their corresponding weight factor. The imaginary part added to the energy is equal to 0.01 Ryd. After summation we perform a standard transformation from the complex to the real energies. All the parameters of our TB-CPA scheme are chosen such that excellent agreement is achieved between our DOS and those obtained within the tetrahedron method of Lehman and Taut [59].

2.3. Total energy calculations

The NTB interpolation scheme is also used to investigate lattice relaxations caused by the presence of a single metal or non-metal vacancy, and to study the atomic and electronic structure properties of the (001) surface. For this purpose, accurate total energy calculations are required. Within our scheme total energy is made of two terms: the first one represents the eigenvalue contribution from the NTB interpolation method (E_{B}), and the second one is a pair-wise potential that accounts for the ion-ion repulsive interactions and the correction to the double counting of the electron-electron interactions. This last term is expressed as [60]

$$V(r) = U_1 \exp[-(r - r_0)/\alpha] + U_2 r_0/r\,, \tag{1}$$

where r is the distance between the neighboring atoms, and U_1, U_2, α, and r_0 are parameters that need to be defined for C–C,C–Ti and Ti–Ti pairs.

The parameters of the potential, see equation 1, are determined from self-consistent pseudo-potential total energy calculations with the plane-wave basis set carried out for crystalline carbon (with FCC and diamond structures), titanium (with FCC and BCC structures) and titanium carbide (with NaCl-type structure for two compositions $TiC_{1.0}$ and $TiC_{0.75}$). We use the local-density approximation to the density functional theory. Norm-conserving pseudo-potentials are constructed according to the Troullier-Martins scheme [61]. The pseudo-potentials are represented in the fully separable form [62] up to $l_{\max} = 2$ and cast into the non-local form for $l = 1, 2$ for Ti and $l = 0, 1$ for C. We adopt the Ceperley-Alder-type exchange-correlation potential [63] as parametrized by Perdew and Zunger [64]. BZ integration is replaced by a sum over a set of 35 special k-points according to the Monkhorst-Pack scheme [65]. The Kohn-Sham plane-wave basis set is truncated at 40 Ryd.

Table 4. Parameters of the repulsive potential.

Denotation	C–C	C–Ti	Ti–Ti
U_1 (Ryd)	–0.67267	–2.58895	–4.47549
U_2 (Ryd)	0.78107	1.59968	4.47158
α	1.91750	4.29714	3.59850
r_0 (Å)	2.12300	2.13100	2.80000

Using the above pseudo-potential procedure, we predict for TiC an equilibrium lattice parameter of 4.262 Å, which is 1.5 % smaller than the experimental value of 4.326 Å [37], and close to the LMTO value of 4.269 Å[25] and 4.258 Å[28]. The calculated bulk modulus (B) for TiC is 303 GPa. This value rather well agrees with the experimental value of 255 GPa [66], and with the result of a previous calculation [25], B = 278 GPa and [28], B = 305 GPa. In figure 1 we show the

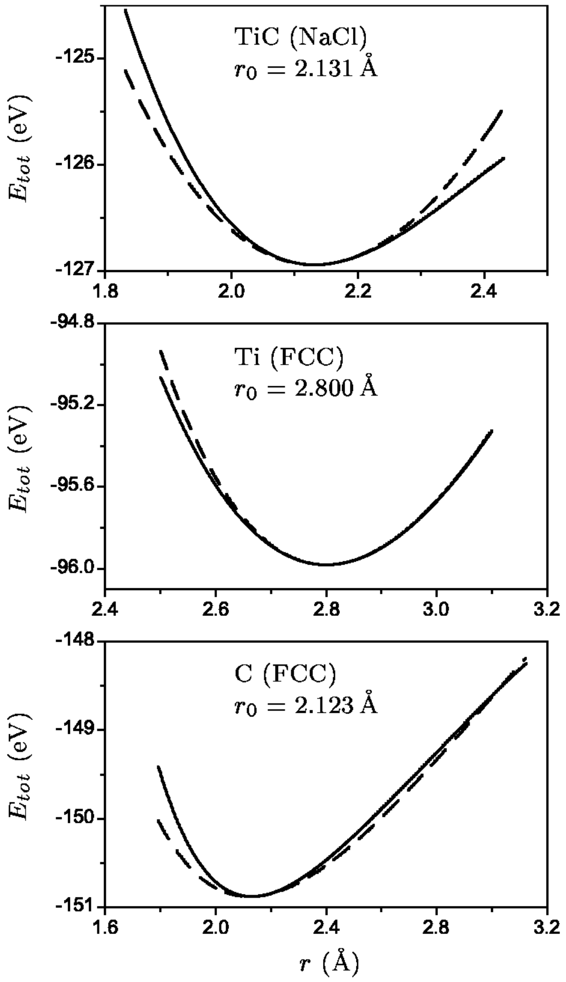

Figure 1. Total energy per atom E_{tot} as a function of inter-atomic distance r determined from the pseudo-potential (solid line) and the TB (dashed line) calculations. r_0 is the equilibrium distance.

total energy results from pseudo-potential and TB calculations for TiC, Ti and C with the FCC structure. First of all, we aimed at correctly approximating the pseudo-potential curves in the equilibrium region of TiC, i.e., around $r \sim 2.131$ Å (Ti–C interactions) and $r \sim 3.014$ Å (C–C and Ti–Ti interactions). Because of some restrictions imposed by the implementation of our TB scheme, we could only calculate the elastic stiffness constants C_{11} and C_{12} for TiC, which were 566 GPa and 172 GPa, respectively, in reasonable agreement with the experimental values of 540 GPa and 110 GPa [66]. Note that in the fitting procedure, the $(R_0/r)^n$ distance dependence of the two-center TB parameters was chosen in accordance with the Harrison rule [67]. The values of n associated with the parameters of the C–Ti block were adjusted to well reproduce the pseudo-potential results for TiC. The complete set of parameters for the NTB interpolation scheme and the repulsive potentials are summarized in tables 2, 3 and 4.

2.4. Structural optimization

The damped Newton dynamics is an efficient and numerical stable method for finding equilibrium geometries. Starting from an initial configuration the nuclei are moved according to the following iterative scheme

$$\mathbf{r^{(n+1)}} = (\mathbf{1} + \lambda_\mathbf{i})\mathbf{r^{(n)}} - \lambda_\mathbf{i}\mathbf{r^{(n-1)}} + \frac{\mathbf{h_i F^{(n)}}}{\mathbf{M_i}}\,, \tag{2}$$

where λ_i, h_i are the damping parameters and M_i is the mass parameter for species $i =$ C, Ti, $\mathbf{F}$ is the force computed from the parametrized TB scheme, and n refers to a specific iteration. The damping parameters determine whether the nuclei slowly lose their initial potential energy in an oscillatory-like motion or they fall quickly into the closest local minimum. In most cases that we simulated, satisfactory self-consistency was achieved under the conditions: $\lambda_i \sim 0$ and $h_i \sim 1$.

The minimization scheme, see equation 2, was used to establish the final atomic configuration of a TiC crystal that contained a single non-metal or metal vacancy. In this case we considered a cubic unit cell of 63 atoms and one vacancy that corresponded to the composition $TiC_{0.97}$. We have also computed the total energy of $TiC_{0.94}$ described by a cubic unit cell of 62 atoms and two non-metal vacancies in different configurations with the intervacancy distances: $a(1/2, 1/2, 0)$ (adjacent), $a(1, 0, 0)$ (opposite) and $a(1, 1, 1)$ (remote). In the case of the TiC (001) surface, we considered a slab of 11 layers with a unit cell of 176 atoms such that each layer of the unit cell contained 8 C atoms and 8 Ti atoms. To check that the slab represents a suitable model for investigating the (001) surface the lower five layers were fixed during the relaxation process. In all the structural optimizations, the iteration process was stopped when the change in the potential energy was less than 10^{-9} eV/atom and the maximal force acting upon an atom did not exceed 10^{-6} eV/Å (3×10^{-4} eV/Å in the case of the 11-layer slab). By computing the Hellmann-Feynman forces only the Γ point was used. Periodic boundary conditions were imposed along three (bulk) or two (surface) directions.

2.5. DOS calculations

After the TB parameters have been fully determined we can effectively calculate the DOS of complex systems, as in our case. Moreover, the NTB interpolation scheme allows us to evaluate charges throughout the unit cell, as opposed to other computational schemes (e.g., APW or LMTO). The DOS calculations were performed for three ordered systems by using the tetrahedron method [59]. The first one is the NaCl-type structure of TiC with two atoms per unit cell. For this structure, the 1/48 part of the BZ was divided into 3430 tetrahedra. The second structure is a 64-atom cubic unit cell, in which case the 1/48 part of the BZ was divided into 456 tetrahedra. Finally, the third system is an 11-layer slab with a 176-atom unit cell. For this system, the irreducible part of the two-dimensional BZ was divided into 64 triangles. The local DOS are computed from the eigenvectors of the generalized eigenvalue problem. Since these eigenvectors are non-orthogonal, their normalization was determined so as to preserve the electro-neutrality of the unit cell.

3. Result and discussion

3.1. Electronic structure of disordered TiC_x

The total and local density of states of TiC obtained for different unit cells are shown in figure 2. The total DOS is very similar to the one calculated by other authors [23–34]. However the local DOS differ from those obtained with a restricted orthogonal TB basis [27] since, in the present study, the Ti s and Ti p states are accounted for. As a consequence we find a net charge transfer of 0.04 electron from the metal to the carbon atoms that is smaller than the one calculated in [27] (1.65 electron). So, according to our model, titanium carbide behaves mostly as a covalent compound.

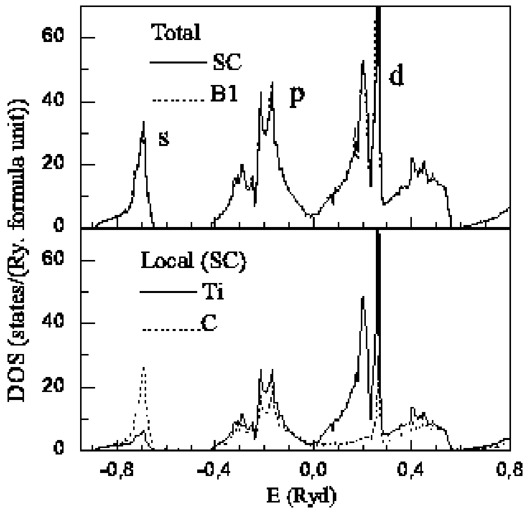

Figure 2. Total and local densities of states of TiC calculated for different structures (SC – simple cubic, B1 – NaCl-type). The Fermi energy is taken as zero of energy.

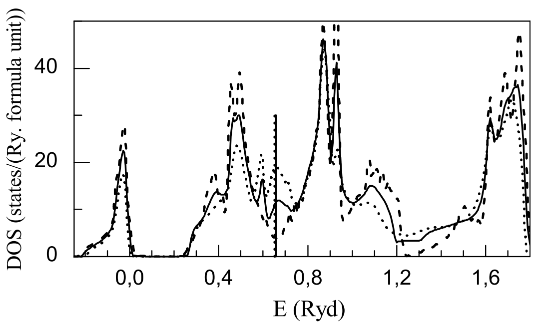

Figure 3. Total TB-CPA densities of states (DOS) of TiC_x for $x = 1.0$ (dashed line), $x = 0.8$ (solid line) and $x = 0.6$ (doted line). The vertical line locates the Fermi energy.

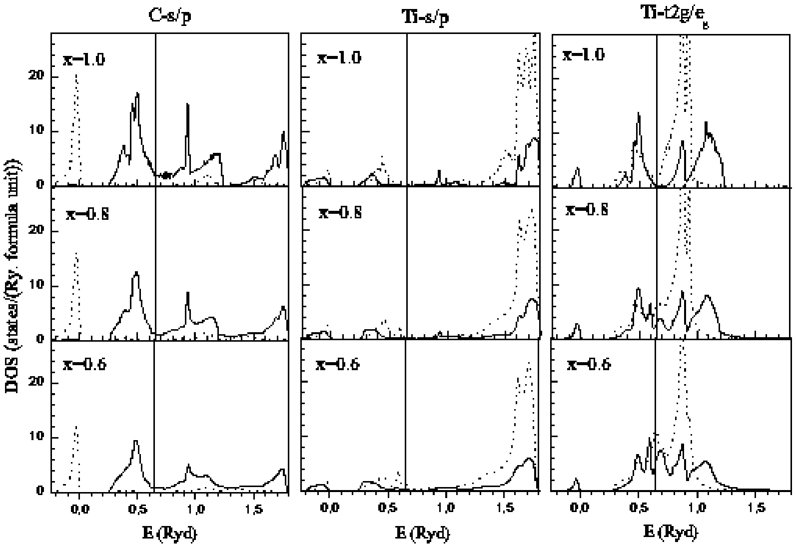

Figure 4. Partial TB-CPA densities of states (DOS) of TiC_x. Left panel: s_C – dashed line, p_C – solid line. Central panel: s_{Ti} – solid line, p_{Ti} – dashed line. Right panel: Ti $d_{t_{2g}}$ $(xy,\ yz,\ zx)$ – dashed line, Ti d_{e_g} $(3z^2 - r^2,\ x^2 - y^2)$ – solid line. The vertical lines locate the Fermi energy.

In figures 3, 4 we present the total and partial DOS of TiC_x, for $x = 1.0$, 0.8, and 0.6 obtained with the NTB-CPA scheme in a wide energy range. The main feature observed in our spectra, as in the KKR-CPA DOS [37], is an increase in the number of states in the Fermi energy region (FER) and a decrease in the C-peak amplitude with decreasing x. At the same time, a redistribution of the Ti e_g states of the p– and d–bands in the FER, and a shift of the Ti t_{2g} and Ti p levels mostly from the p–band to the FER are observed. It is clearly seen that the band gap around 1.25 Ryd vanishes with an increase in the number of C-vacancies. Such a redistribution of the

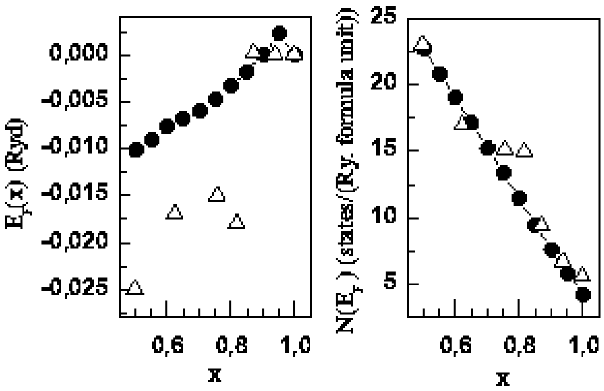

Figure 5. The Fermi energy, E_F, and the density of states at the Fermi energy, $N(E_F)$, as functions of carbon concentration, x, in TiC_x. Solid circles – our data, open triangles – the results of reference [37].

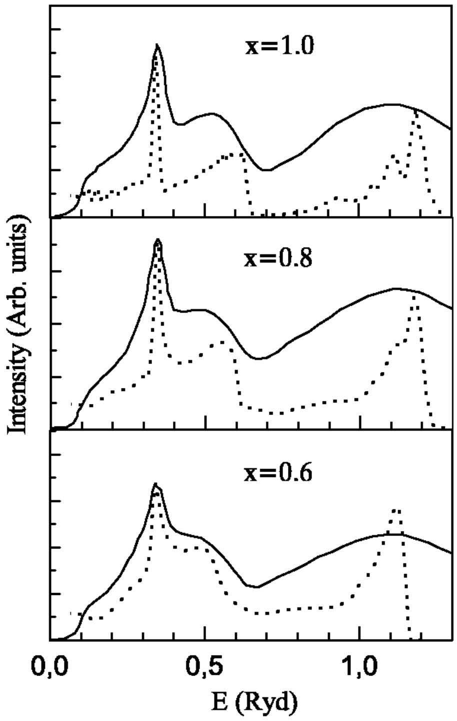

Figure 6. Results of the comparison for the unoccupied part of the TB-CPA p_{C}–DOS (dashed line) with the X-ray C K_α absorption spectra [68] (solid line) for TiC_x.

valence states points to a weakening of the (C p)–(Ti e_g) ($pd\sigma$) and (C p)–(Ti t_{2g}) ($pd\pi$) bonds, and to a strengthening of the Ti–Ti ones. In figure 5 we compare the concentration dependence of the Fermi energy and DOS at E_{F}, $N(E_{\mathrm{F}})$, obtained in our work and in [37]. One can see that, according to our results, the Fermi energy slowly decreases, and $N(E_{\mathrm{F}})$ increases with the increasing x. The concentration dependence [37] of these two quantities shows a plateau around $x = 0.8$. The causes of this anomaly were discussed above. Since we have not found any evidence for the extremal concentration dependence of the kinetic characteristics in disordered TiC_x [1–3], our scheme seems to be more suitable for the description of the kinetic properties than the approach [37]. To verify the reliability of our procedure we compared the unoccupied part of the C p DOS with the X-ray C K_α absorption spectra of TiC_x [68]. The results of such comparisons are presented in figure 6. We have also calculated the X-ray Ti L_{III} and Ti $K_{\beta 5}$ emission spectra according to the procedure of Klima [36]. The calculated spectra were smoothed out by convoluting the DOS with a Lorentzian function, and by taking into account an intrinsic level width of about 0.05 eV and an experimental spectral resolution of about 0.04 eV [22]. These spectra were selected since they are associated with the Ti d and p DOS that are the most effected by C-vacancies. The calculated and experimental spectra [22,69] displayed in figure 7 show that the main features observed experimentally are properly reproduced.

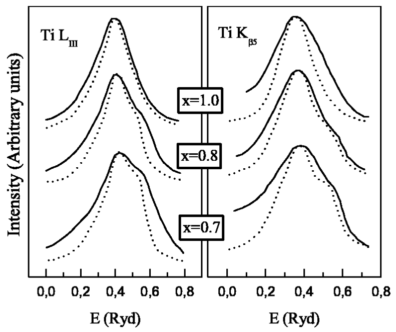

Figure 7. Calculated (dashed line) and experimental (solid line) X-ray emission spectra [22,69] for TiC_x.

As mentioned earlier, the orthogonal TB interpolation schemes applied to TiC_x [36] and other similar compounds [57,58] have failed to reproduce the redistribution of valence states caused by the presence of non-metal vacancies. In particular, the main changes in the DOS related to non-metal vacancies lead to a shift of the Fermi level toward higher energies, and to a reduction of the carbon peaks. Now it is clear that such effects are associated with the neglect of overlap matrix effects in the TB computational procedure. Since for TiC the overlap and hopping integrals turned out to be comparable (cf. table 2, 3) the electronic properties of the transition metal compounds can be correctly described provided a non-orthogonal TB basis is used. It is worth mentioning that this complication is not necessary in the case of SiC (as well as similar compounds), for which the properties are correctly described in the framework of an orthogonal TB scheme [70].

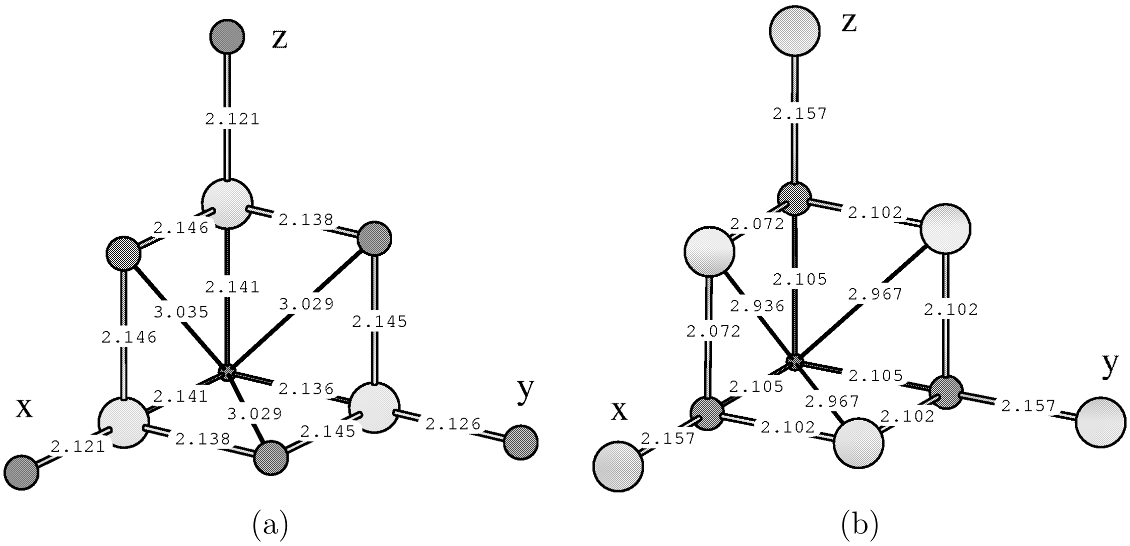

Figure 8. Lattice relaxations around a C-vacancy (a) and a Ti-vacancy (b). The numbers denote bond-lengths (in Å). Small, medium and large spheres refer to C(Ti)–vacancy, C and Ti atoms, respectively.

Table 5. Equilibrium lattice parameters (a_0), maximal outward shifts of the atoms around the vacancy (d), total energy (E_{T}) of the relaxed and non-relaxed $\mathrm{Ti}_n\mathrm{C}_m$ crystals.

	Vacancy config.	Non-Relaxed	
		a_0 (Å)	E_{T} (eV/atom)
$Ti_{32}C_{32}$	—	4.262	−19.257152
$Ti_{32}C_{31}$	—	4.2635	−18.764040
$Ti_{32}C_{30}$	adjacent	4.264	−18.227195
	opposite	4.265	−18.237913
	remote	4.264	−18.267252
$Ti_{31}C_{32}$	—	4.257	−18.237174

	Vacancy config.	Relaxed		d (Å)
		a_0 (Å)	E_{T} (eV/atom)	
$Ti_{32}C_{32}$	—	—	—	0.000
$Ti_{32}C_{31}$	—	4.2635	−18.765394	0.010
$Ti_{32}C_{30}$	adjacent	4.264	−18.229977	0.090
	opposite	4.266	−18.241169	0.018
	remote	4.266	−18.270507	0.018
$Ti_{31}C_{32}$	—	4.257	−18.245515	0.026

3.2. Static lattice relaxation around vacancies

The atomic configurations around the single non-metal and metal vacancies determined as a result of the structure optimization based on the parametrized TB scheme are shown in figure 8. While in TiC the equilibrium C–Ti and C–C (Ti–Ti) distances are 2.131 Å and 3.014 Å, respectively, in $TiC_{0.97}$ the V_{C}–Ti distances are 2.136 Å along the y-axis and 2.141 Å along the x- and z-axis, and the V_{C}–C distances are 3.035 Å in the x-z plane and 3.029 Å in the x-y and z-y planes (figure 8a). The SNN atoms shift outward around the V_{C} in the corresponding planes. The third nearest neighbor atoms shift toward the V_{C} (not shown in figure 8). The change in the total energy per atom between relaxed $TiC_{0.97}$ and unrelaxed TiC is 0.492 eV/atom, and the energetic gain due to relaxation is 0.001 eV/atom.

In the case of a metal vacancy, we obtained the following rearrangement of the atoms around V_{Ti}. In $Ti_{0.97}C$ all the V_{Ti}–C distances are 2.105 Å whereas the V_{Ti}–Ti distances are 2.936 Å in the x-z plane and 2.967 Å in the x-y and z-y planes (figure 8b). Hence, homogeneous inward relaxation of the FNN atoms and inhomogeneous inward shift of the SNN atoms take place around the metal vacancy. The third nearest neighbor atoms shift outward around V_{Ti} (not shown in figure 8). In the sequence TiC – non-relaxed $Ti_{0.97}C$ – relaxed $Ti_{0.97}C$, E_{T} changes are $0.000 - 1.020 - 1.012$ eV/atom. (The zero of E_{T} refers to the total energy of the stoichiometric compound).

So far, we considered the atomic relaxation around the single non-metal and metal vacancies in titanium carbide with the equilibrium lattice parameter equal to that of TiC (4.262 Å). Along with these investigations, we have carried out the structural optimization in which the changes in the lattice parameters were taken into account. Characteristics of the non-relaxed and relaxed structures with the single and two vacancies for the equilibrium lattice parameters are summarized in table 5. One can see that the equilibrium lattice parameter increases with the increasing non-metal vacancy concentration. For the single metal vacancy we have the opposite picture. The values of the relaxations are independent of the lattice parameter. For the crystal with two non-metal vacancies the equilibrium lattice parameter depends on the vacancy configuration. But in all the cases, for the small vacancy compositions our TB model gives the lattice expansion with the decreasing carbon content, in agreement with the experiment [1,2,4].

In summary, one can infer that non-metal vacancies are more energetically favored than metal vacancies. We also established that, in TiC_x, for $x > 0.94$, the remote vacancy configuration is preferable as compared to the configurations with the opposite or adjacent non-metal vacancies in good agreement with the findings of structural investigations of substoichiometric transition metal compounds [1,2,4,9]. In contrast to previous results [25,44,46], we find for TiC an inhomogeneous tetragonal outward relaxation of the Ti and C atoms around the C-vacancy. Such a situation has been confirmed in TiN, VN [20,46] and NbC [3]. As seen in figure 4, the creation of the non-metal vacancies leads to the appearance of the d-vacancy states at the Fermi level. Therefore, the energy of the system can be lowered due to the splitting of the vacancy levels (the Jahn-Teller theorem) caused by a lattice distortion. So, the lattice distortion that accompanies atomic relaxation can take place provided the vacancy states are formed in the Fermi level region. Namely, such a situation is realized in TiC_x according to our calculations and other experimental and theoretical investigations [3,26,30,32]. If one allows for the tendency of increasing the outward relaxation with the increasing number of non-metal vacancies (table 1), the values of the atomic shifts of about 0.010 and 0.018 Å for $TiC_{0.97}$ and $TiC_{0.94}$, respectively, seem to be reasonably correlated with the analogous experimental [7,9–11] and theoretical [26] values for TiC_x, $0.5 < x < 0.76$. As mentioned earlier, previous calculations [25,44,46] also found an outward uniform relaxation but with higher values.

Table 6. Mean interlayer distances, d_{i-j} between i and j layers, and difference in the shifts of C and Ti atoms in the same layer along the z-direction, ΔR_i, in the symmetrical and asymmetrical slabs (in Å). The surface layer is numbered as 1. (The theoretical FNN distance in TiC is 2.131 Å).

Slab	d_{1-2}	d_{2-3}	d_{3-4}	d_{4-5}	d_{5-6}
Sym.	2.097	2.162	2.142	2.138	2.136
Asym.	2.100	2.149	2.149	2.139	2.135

Slab	ΔR_1	ΔR_2	ΔR_3	ΔR_4	ΔR_5	ΔR_6
Sym.	0.136	0.128	0.079	0.077	0.037	0.000
Asym.	0.138	0.115	0.091	0.072	0.036	0.006

3.3. Atomic and electronic structures of the TiC (001) surface layers

Since, so far, the relaxation of the intrinsic layers in the TiC (001) slabs was studied incompletely, one of the tasks in studying the surface layers of TiC was to determine the lattice relaxations inside the (001) slab. In table 6 we show the mean interlayer distances and the distances between the C and Ti atoms in the same layer along the z-direction in the first six layers of the 11-layer symmetrical and asymmetrical slabs obtained with the optimization process described by equation 2. The relaxation occurs predominantly in the direction perpendicular to the surface (z-direction). The surface carbon atoms shift towards the bulk. All other carbon atoms move outward from the central layers. The carbon and titanium atoms belonging to the same layer shift in opposite directions. Correspondingly, all the titanium atoms shift in the directions opposite to those of the carbon displacements. In particular,

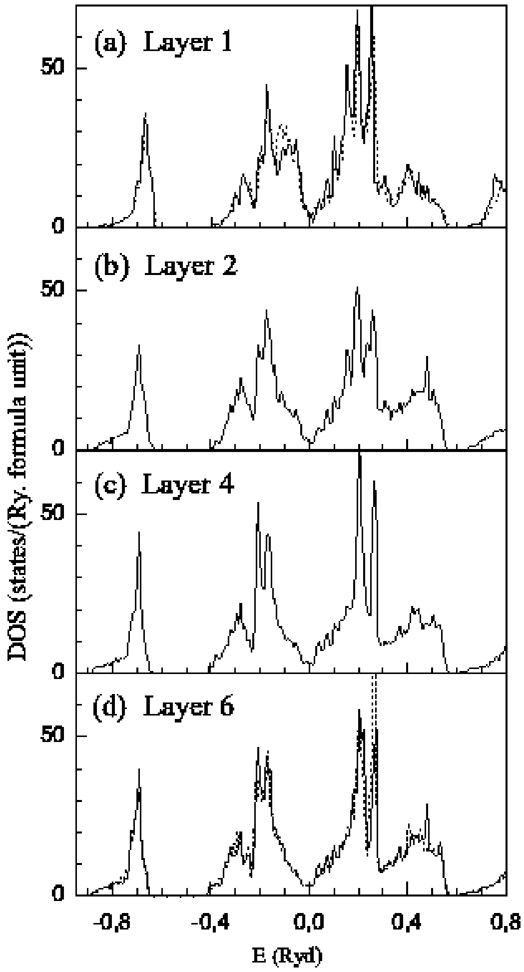

Figure 9. Layer-projected densities of states (DOS) of the symmetrical slab (solid line); DOS of the (001) surface of the unrelaxed 11-layer slab: a, dashed line; DOS of the central layer of the relaxed slab: d, dashed line. The Fermi energy is taken as zero of energy.

the surface titanium atoms move outward from the bulk, and all the other Ti atoms shift towards the central layer. To verify whether such atomic shifts are not related to the symmetry of the slab we performed similar calculations for an asymmetrical 11-layer slab in which the lower five layers are fixed during the structural optimization. One can see that the atomic relaxations in both slabs are similar. Therefore, the established character of the lattice distortions is not the effect of the slab symmetry, but is only related to the geometry of the TiC (001) surface. Obviously, the distortion amplitude reduces towards the central layer. The results of table 6 point to a decrease in the distances when approaching the central layer. From table 6 it is also observed that the outer surface layer is pushed toward the bulk region. The interlayer distances in the central layer slightly differ from those in the bulk, which implies that the atomic distortions should cancel beyond the sixth layer.

The layer-projected DOS of the symmetrical slab are shown in figure 9 whereas the partial DOS of the surface and central layers are compared in figure 10.

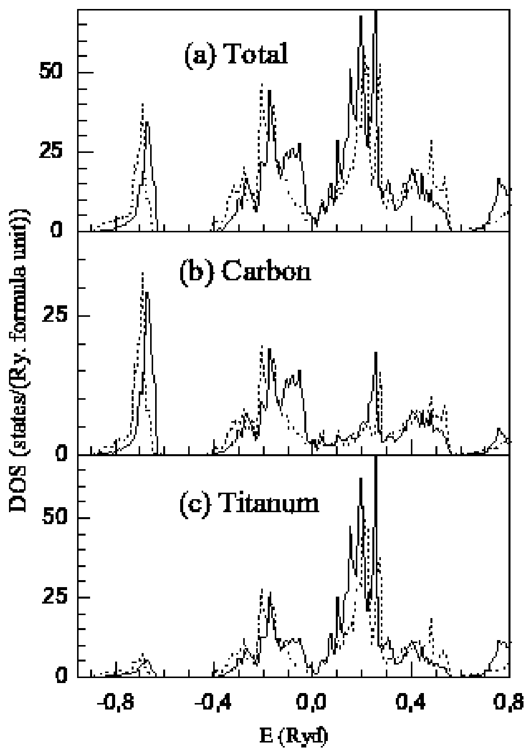

Figure 10. Total (a) and partial (b and c) DOS of the surface (solid line) and central (dashed line) layers in the 11-layer relaxed symmetrical slab. The Fermi energy is taken as zero of energy.

Obviously the layer-projected electronic spectra become more similar to the bulk DOS when approaching the central layer from the surface, and the largest changes occur for the surface spectrum. First of all we reveal the energy shift of the surface DOS towards higher energies as compared to that of the central layer by about 0.02 Ryd, in agreement with the results [47–49,51]. However, we also identify surface resonance states which show up as additional peaks in the DOS at the right-end side of the p-peak (around -0.1 Ryd) and at the left-end side of the d-peak (around $+0.15$ Ryd). For comparison, one notes that similar electronic features at -0.11 Ryd and $+0.14$ Ryd were also reported in references [48,49]. Moreover, from our results, the main peaks of the p- and d-bands get closer. These modifications in the surface DOS clearly point to the occurrence of a new type of interactions that are absent in the bulk. Part of the strong bulk (C p)–(Ti d) bonds are weakened near the (001) surface and this consequently affects the surface electronic spectrum. We should emphasize the fact that besides the C–Ti interactions, other types of interactions also appear at the surface, but their impact on the DOS is minimal. The appearance of SRS leads to a shift in the Fermi energy to a lower energy, or to a shift of the surface DOS at higher energies with reference to the DOS associated with the central layer. Based on these findings, we suggest that the peaks around -0.1 Ryd and -0.21 Ryd in the angle-resolved photo-electron spectra of the TiC (001) [15] and TiN (001) [16] are caused by SRS.

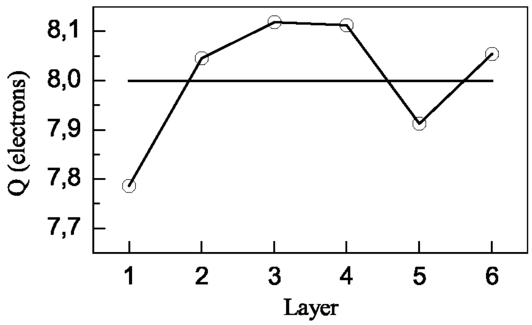

Figure 11. Average charge per layer and per formula unit $Q = \int^{E_\mathrm{F}} N(E)\mathrm{d}E$ in the relaxed 11-layer symmetrical slab. The horizontal line denotes the average charge in the bulk.

The results presented in figure 10 allow us to analyze the effect of relaxation on the surface DOS. The surface and bulk relaxations promote the saturation of weak bonds in the surface region which leads to a reduction in the number of SRS around -0.1 Ryd in the relaxed DOS as compared with the unrelaxed one. As a result, the average band energy of the relaxed surface is lower than that of the unrelaxed surface by about 0.1 Ryd. The values of E_B related to other layers are comparable for the relaxed and unrelaxed slabs. The analysis of the modification of the DOS (figure 9) shows that one should expect that the layer-projected total charge localized at the surface atoms will be smaller than that in the buried layers. In figure 11 we show the average charges normalized per formula unit centered on different layers in the symmetrical slab. One can see that the charge sharply increases from the surface to the buried layers until bulk behavior is reached. Such a change in the atomic charge states correlates well with the interlayer displacements d_{i-j} in the slabs (cf. table 6). In particular, we observe that the distance d_{1-2} is much smaller than any other interlayer distance. Based on the electronic structure analysis we should expect that the atoms, that are inside the slabs restricted by the (001) planes, move during the relaxation process to reduce the number of SRS and the charge of the outer layer to minimize the band energy E_B of the system. The relaxation of C and Ti surface atoms when compared with the unrelaxed surface ones are 0.048 Å towards the bulk and 0.088 Å outward the bulk, respectively. So, the rumpling relaxation is slightly higher as compared with that obtained by Aono et al. [13], according to which the C and Ti atoms of the surface layer are coplanar within the range ± 0.1 Å. Our conclusion is consistent with the results of Wimmer, Neckel and Freeman [49] and Tan et al. [44], which predict the inward and outward relaxation for the C and Ti surface atoms, respectively. Our findings do not confirm the carbon-out and titanium-in relaxation found by Price, Wills and Cooper [53] and Kobayashi [54].

4. Conclusions

Results were presented for off-stoichiometric titanium carbides described with a disordered non-metal sub-lattice, TiC structures with single vacancies, and 11-layer slabs. The investigations have been carried out within a parameterized non-orthogonal tight-binding scheme. The validation of some of our conclusions with available experimental data and past theoretical results, clearly confirms the reliability of the computational procedure. It has been shown that earlier variants of the TB methodology have failed to reproduce salient features of the electronic structure of off-stoichiometric transition metal compounds because of the neglect of the overlap matrix elements in the TB Hamiltonian. The TB-CPA DOS of TiC_x show that the electronic states of the transition metal are redistributed from the d–band to the Fermi level region with the decreasing x, and this causes a shift of the Fermi level towards low energies, and an increase in the DOS at E_F. The structural optimization calculations have shown that the FNN and SNN atoms of a single non-metal vacancy tetragonally shift away from the vacancy, whereas, in the case of a metal vacancy, the FNN carbon atoms relax homogeneously toward the vacancy and the SNN metal atoms move inhomogeneously toward the vacancy. Our model predicts that the off-stoichiometric composition with the remote vacancy configuration is more energetically favored than the configurations having opposite and adjacent non-metal vacancies. The analysis of the atomic relaxations in the 11-layer slabs restricted by a (001) plane shows that the C and Ti surface atoms shift inward and outward, respectively. The amplitude of the shifts decreases rapidly with the distance from the surface layer, and the surface atoms move toward the bulk layers. The relaxations of the 11-layer slabs lead to a reduction in the number of surface resonance states and in the charge of the outer layer, and this promotes a reduction in the band energy contribution to the total energy of the system. The present methodology will be applied in a near future to the study of ordered off-stoichiometric titanium carbides.

This work was supported in part under the STCU Contract No. 1591. The work of P. T. was performed under the auspices of U. S. Department of Energy by the University of California Lawrence Livermore National Laboratory under Contract No. W-7405-ENG-48.

References

1. Toth L.A. Transition Metal Carbides and Nitrides. New York, 1971.
2. Freer R. (ed.) The Physics and Chemistry of Carbides, Nitrides and Borides. Dordrecht, 1990.
3. Gubanov V.A., Ivanovsky A.L., Zhukov V.P. Electronic Structure of Refractory Carbides and Nitrides. Cambridge, 1994.
4. Gusev A.I., Rempel A.A., Nagerl A.J. Disorder and Order in Strongly Nonstoichiometric Compounds. Berlin, 2001.
5. Lipatnikov V.N., Kottar A., Zueva L.V., Gusev A.I. // Neorg. Mater., 2000, vol. 36, p. 206.
6. de Novion C.H., Landesman J.P. // Pure Appl. Chem., 1985, vol. 57, p. 1391.
7. Moisy-Maurice V., de Novion C.H., Christensen A.N., Just W. // Solid State Commun., 1981, vol. 39, p. 661.
8. Dunand A., Flack H.D., Yvon K. // Phys. Rev. B, 1990, vol. 31, p. 2299.
9. Priem T., Beunen B., de Novion C.H., Chevrier J., Livet J.F., Finel A. // Physica B, 1989, vol. 156–7, p. 47.
10. Moisy-Maurice V., Novion C.H. // J. Physique, 1988, vol. 49, p. 1737.
11. Goretski H. // Phys. Status Solidi, 1967, vol. 20, p. K141.
12. Nakagura S., Kusunoki T. // J. Appl. Crystallogr., 1977, vol. 10, p. 52.
13. Aono M., Hou Y., Souda R., Oshima C., Otani S., Ishizawa Y. // Phys. Rev. Lett., 1983, vol. 50, p. 1293.
14. Bradshaw A.M., van der Veen J.F., Himpsel F.J., Eastman D.E. // Solid State Commun., 1980, vol. 37, p. 37.
15. Callenas A., Johansson L.I., Christensen A.N., Schwartz K., Redinger J. // Phys. Rev. B, 1983, vol. 27, p. 5934.
16. Johansson L.I., Callenas A. // Solid State Commun., 1982, vol. 42, p. 299.
17. Calais J.-L. // Adv. Phys., 1977, vol. 26, p. 847.
18. Neckel A. // Int. J. Quantum Chem., 1983, vol. 23, p. 1317.
19. Schwarz K. // CRC Crut. Rev. Solid State Mater. Sci., 1987, vol. 13, p. 211.
20. Skala L., Capkova P. // J. Phys.: Condens. Matter, 1990, vol. 2, p. 8293.
21. Koide T., Shidara T., Fukurani H., Fujimori A., Miyahara T., Kato H., Otani S., Ishizava Y. // Phys. Rev. B, 1990, vol. 42, p. 4979.
22. Gubanov V.A., Kurmaev E.Z., Ellis D.E. // J. Phys. C, 1981, vol. 14, p. 5567.
23. Ahuja R., Eriksson O., Wills J.M., Johansson B. // Phys. Rev. B, 1996, vol. 53, p. 3072.
24. Scott A.J., Brydson R. // Phys. Rev. B, 2001, vol. 63, p. 245105.
25. Hugosson H.W., Korzhavyi P., Johansson U., Jansson D., Eriksson O. // Phys. Rev. B, 2001, vol. 63, p. 165116.
26. Eibler R. // J. Phys.: Condens. Matter, 2002, vol. 14, p. 4425.
27. Neckel A., Rastl P., Eibler R., Weinberger P., Schwarz K. // J. Phys. C, 1976, vol. 9, p. 579.
28. Zhukov V.P., Gubanov V.A., Jepsen O., Christensen N.E. // J. Phys. Chem. Solids, 1988, vol. 49, p. 841.
29. Haglund J., Crimvall G., Jarlborg T., Guillermet A.F. // Phys. Rev. B, 1991, vol. 43, p. 14400.
30. Guemmaz M., Moraitis G., Mosser A., Khan M.A., Parlebas J.C. // J. Alloys and

Compounds, 1997, vol. 262-, p. 397.
31. Jhi C.-H., Ihm J. // Phys. Rev. B, 1997, vol. 56, p. 13826.
32. Grossman J.C., Nizel A., Cote M., Cohen M.L., Louie S.G. // Phys. Rev. B, 1999, vol. 60, p. 6343.
33. Jhi C.-H., Ihm J., Louie S.G., Cohen M.L. // Nature, 1999, vol. 339, p. 132.
34. Louie C.-H., Jhi S.G., Cohen M.L., Morris J.W. // Phys. Rev. Lett., 2001, vol. 87, p. 075503.
35. Huisman L.M., Carlson A.E., Gellatt C.D. // Phys. Rev. B, 1980, vol. 22, p. 991.
36. Klima J. // J. Phys. C, 1979, vol. 12, p. 3691.
37. Marksteiner P., Weinberger P., Neckel A., Zeller R., Dederichs P.H. // Phys. Rev. B, 1986, vol. 33, p. 812.
38. Landesman J.P., Tréglia G., Turchi P., Ducastelle F. // J. Phys. (Paris), 1985, vol. 46, p. 1001.
39. Redinger J., Eibler R., Herzig P., Neckel A., Podloucky R., Wimmer E. // J. Phys. Chem. Solids, 1985, vol. 46, p. 383.
40. Redinger J., Eibler R., Herzig P., Neckel A., Podloucky R., Wimmer E. // J. Phys. Chem. Solids, 1986, vol. 47, p. 387.
41. Zhukov V.P., Gubanov V.A. // J. Phys. Chem. Solids, 1987, vol. 48, p. 187.
42. Puska M.J., Sob M., Braurer G., Korhonen T. // Phys. Rev. B, 1994, vol. 49, p. 10947.
43. Guemmaz M., Moraitis G., Mosser A., Khan M.A., Parlebas J.C. // J. Electron Spectrosc. Relat. Phenom., 1997, vol. 83, p. 173.
44. Tan K.E., Bratkovsky A.M., Harris R.M., Horsfield A.P, Nguen-Mahn D., Pettifor D.G., Sutton A.P. // Modell. Simul. Mater. Sci. Eng., 1997, vol. 5, p. 187.
45. Korzhavyi P.A., Porouskii L., Hugosson H.W., Ruban A.V., Johansson B. // Phys. Rev. Lett., 2002, vol. 88, p. 015505.
46. Capkova P., Skala L. // Phys. Stat. Solidi (b), 1992, vol. 171, p. 85.
47. Fujimori A., Minanu F., Tsudo N. // Surface Sci., 1982, vol. 121, p. 199.
48. Wimmer E. // J. Phys. C, 1984, vol. 17, p. L365.
49. Wimmer E., Neckel A., Freeman A.J. // Phys. Rev. B, 1985, vol. 31, p. 2370.
50. Tan K.E., Horsfield A.P, Mahn D.N., Pettifor D.G., Sutton A.P. // Phys. Rev. Lett., 1996, vol. 76, p. 90.
51. Price D.L., Cooper B.R., Wills J.M. // Phys. Rev. B, 1992, vol. 46, p. 11368.
52. Price D.L., Wills J.M., Cooper B.R. // Phys. Rev. B, 1993, vol. 48, p. 15301.
53. Price D.L., Wills J.M., Cooper B.R. // Phys. Rev. Lett., 1996, vol. 77, p. 3375.
54. Kobayashi K. // Jpn. J. Appl. Phys., 2000, vol. 39, p. 4311.
55. Mattheis L.F. // Phys. Rev. B, 1972, vol. 5, p. 290.
56. Faulkner J.S. // Phys. Rev. B, 1976, vol. 13, p. 2391.
57. Klein B.M., Papaconstantopoulos D.A., Boyer L. // Phys. Rev. B, 1980, vol. 22, p. 1946.
58. Klima J. // Czech. J. Phys. B, 1980, vol. 30, p. 905.
59. Lehman J., Taut M. // Phys. Status Solidi (b), 1972, vol. 54, p. 469.
60. Molteni C., Colombo L., Miglio L. // Phys. Rev. B, 1994, vol. 50, p. 4371.
61. Troullier N., Martins J.L. // Phys. Rev. B, 1991, vol. 43, p. 1993.
62. Kleinman L., Bylander D.M. // Phys. Rev. Lett., 1982, vol. 48, p. 1425.
63. Ceperley D.M., Alder S.J. // Phys. Rev. Lett., 1980, vol. 45, p. 566.
64. Perdew J.P., Zunger A. // Phys. Rev. B, 1981, vol. 23, p. 5048.
65. Monkhorst H.J., Pack J.D. // Phys. Rev. B, 1976, vol. 13, p. 5188.

66. Pintschovius L., Reichardt W., Scheerer B. // J. Phys. C, 1978, vol. 11, p. 1557.
67. Harrison W.A. Elecronic Structure and Properties of Solids. San Francisco, 1980.
68. Pfluger J., Fink J., Grecelius G., Bohnen K.P., Winter H. // Solid State Commun., 1982, vol. 44, p. 489.
69. Kindrat M. Ph. D. Thesis. Institute of Metal Physics. Kyiv, Ukraine, 1982.
70. Ivashchenko V.I., Turchi P. E.A., Shevchenko V.I., Ivashchenko L.A., Rusakov G.V. // Phys. Rev. B, 2002, vol. 66, p. 195201.

Дослідження TiC_x в наближенні сильного зв'язку

В.І.Іващенко [1], П.Е.А.Турчі [2], В.І.Шевченко [1], Л.А.Іващенко [1], О.К.Порада [1]

[1] Інститут проблем матеріалознавства, НАН України, вул. Кржижановського 3, 03142 Київ, Україна

[2] Ліверморська національна лаболаторія Лоуренса (L-353), P.O. Box 808, Livermore, CA 94551, USA

Отримано 8 грудня 2003 р.

Параметризований неортогональний метод сильного зв'язку (СЗ), а також наближення когерентного потенціалу застосовано до вивчення електронної структури розупорядкованого нестехіометричного TiC_x, релаксації ґратки та електронного спектру поверхні (001) TiC, локальних релаксацій та енергетичних станів структур TiC, які містять одну або дві вакансії як в неметалевій, так і в металевій підґратках. Результати розрахунків добре узгоджуються з існуючими експериментальними та теоретичними даними. Продемонстрована важливість врахування матричних елементів перекриття гамільтоніану для опису електронної структури цього класу сполук.

Ключові слова: *карбід титану, неортогональна модель сильного зв'язку, поодинока вакансія, релаксація поверхні*

PACS: *71.20.B, 61.72.J, 68.35.B*